JACS
JOURNAL OF THE AMERICAN CHEMICAL SOCIETY
pubs.acs.org/JACS
Article

Decompression-Induced Chemical Reaction in CL-20

Xin Zhang,[▽] Kaiyuan Shi,[▽] Jian Xu,[▽] Fengyuan Shi,[▽] Jian Wang, Jiaqing Zhang, Xingbang Dong, Jun Kong, Zhaoxu Du, Haotian Yang, Xiao Dong,* Jun Chen,* Wanghua Chen,* and Lei Su*

Cite This: J. Am. Chem. Soc. 2025, 147, 24759−24765
Read Online
ACCESS | Metrics & More | Article Recommendations | Supporting Information

ABSTRACT: Energetic materials have closely correlated safety and high-pressure chemical reaction kinetics. While extensive research has typically focused on structural evolution and reversible phase transitions at high pressures, chemical decomposition pathways remain underexplored. Here, we report a novel pressure-induced chemical reaction in CL-20 during decompression from a peak pressure of 26.2 GPa under nonhydrostatic compression. Infrared spectroscopy confirmed chemical bond cleavage, yielding gaseous decomposition products primarily composed of N_2O and CO_2. Molecular dynamics simulations revealed that the initial decomposition steps involved H migration, OH transfer, β-scission of the C−C bridge, and cleavage of C−N bonds. Notably, under improved hydrostatic conditions (using KBr as the pressure-transmitting medium), the reaction threshold pressure increased to 30.1 GPa, highlighting the critical roles of shear stress in the diamond anvil cell environment. This study represents the first clear demonstration of decompression-induced chemical reactions in condensed explosives, providing fundamental insights into their intrinsic safety mechanisms as well as their initiation and detonation behaviors.

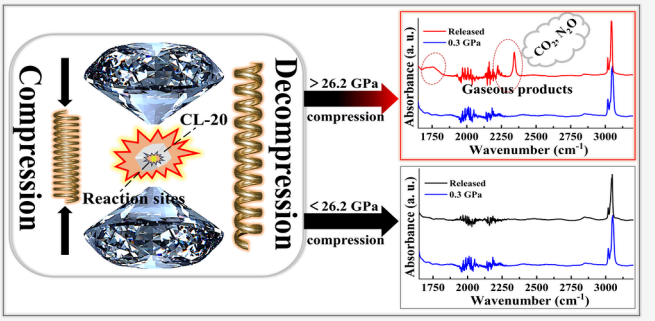

INTRODUCTION

Energetic materials (EMs) are characterized by their ability to rapidly release chemical energy through the conversion of reactants to gaseous products under external stimuli. This distinctive property makes them indispensable in numerous fields, including defense, aerospace propulsion, mining, and industrial applications.[1−3] Despite extensive research efforts, the precise reaction mechanisms and underlying chemical dynamics governing EMs' decomposition under extreme conditions—particularly involving simultaneous high-temperature and high-pressure environments—remain poorly understood.[4−10] Understanding the reactivity mechanism of EMs is vital not only for the accurate prediction of EM sensitivity but also for advancing the development of next-generation materials with optimized performance and enhanced safety.[11]

Due to the extremely transient nature of explosive reactions—which simultaneously involve intense pressures and temperatures—disentangling the individual effects of temperature and pressure on chemical reactivity has historically been challenging.[12,13] Clearly isolating pressure effects from thermal contributions is therefore crucial for gaining fundamental insights into EM decomposition mechanisms and intrinsic sensitivity under mechanical loading.[14] Traditionally, temperature has been widely recognized as the primary driver of chemical reactions in EMs, particularly for well-studied compounds such as 1,3,5,7-tetranitro-1,3,5,7-tetrazocine ($C_3H_3N_6O_6$, HMX), 1,3,5-trinitro-1,3,5-triazacyclohexane ($C_4H_8N_8O_8$, RDX), and hexanitro-hexaazaisowurtzitane ($C_6H_6N_{12}O_{12}$, CL-20).[15] In fact, molecules expand at elevated temperatures, resulting in increased intermolecular distances and facilitating the cleavage of chemical bonds. At present, N-NO_2 cleavage predominantly occurs in the early stages of the thermal decomposition of HMX, RDX, and CL-20.[16−20] Such processes typically produce gaseous species including NO_2, NO, CO, CH_2O, HCN, H_2O, N_2O, and CO_2. Moreover, recent molecular dynamics (MD) simulations have revealed that the thermal decomposition pathways of CL-20 depend significantly on reaction conditions, with multiple initiation mechanisms potentially occurring simultaneously.[21−23]

Beyond thermal effects, pressure has recently emerged as another critical factor influencing chemical reactivity, primarily through enhanced molecular aggregation, structural rearrangements, and even polymerization reactions, as widely documented in unsaturated hydrocarbons such as benzene, acetylene, ethylene, and butadiene.[24−28] However, most energetic materials, which typically feature saturated structures, exhibit remarkable chemical stability under pressure, and existing high-pressure studies have predominantly focused on structural phase transitions rather than chemical decomposi-

Received: April 15, 2025
Revised: June 24, 2025
Accepted: June 25, 2025
Published: July 2, 2025

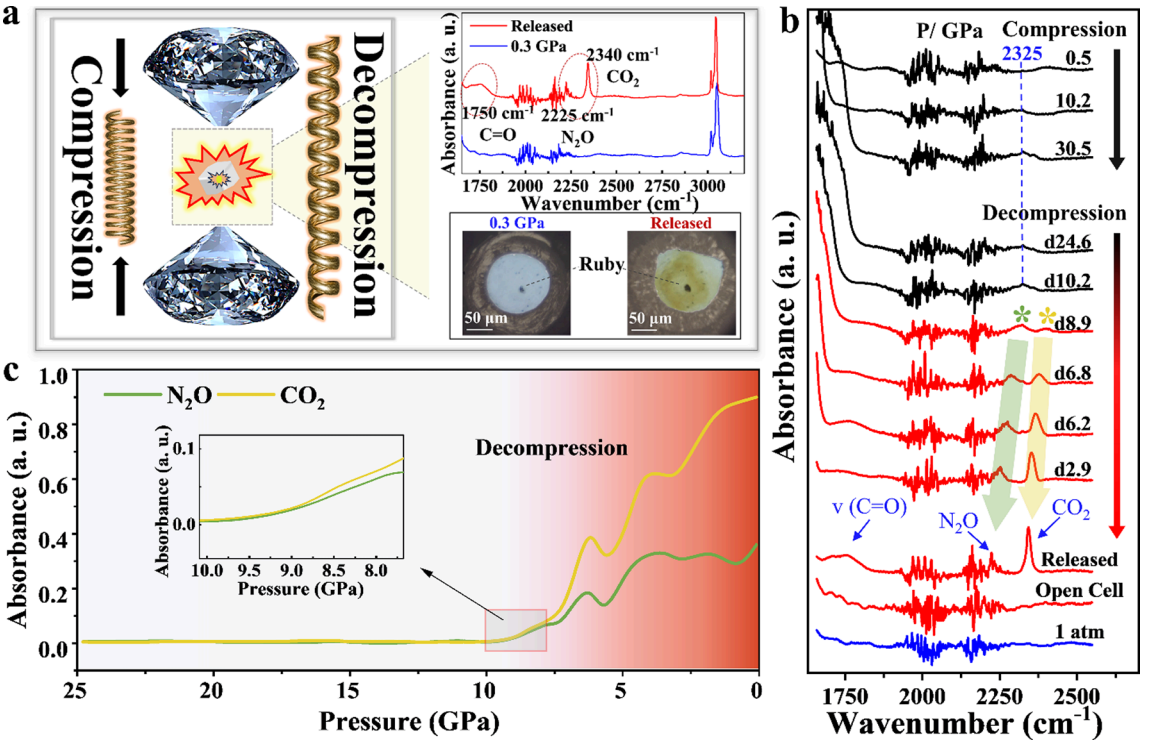

Figure 1. Chemical reaction of CL-20 after the compression−decompression cycle under nonhydrostatic pressure conditions. (a) IR spectra and corresponding optical micrographs of CL-20 before and after the pressure treatment. The in situ images at 0.3 and 0 GPa (released) were included to visually demonstrate the color change of the CL-20 crystal before compression and after decompression. The dotted ellipses represent the IR peaks of the decomposition products. (b) In situ high-pressure IR spectra from 1600 to 2550 cm^{-1} at different pressures. The dashed line represents the IR peaks of the CO_2 IR peak in the air (2325 cm^{-1}). The blue arrows mark the new peaks. ν represents the stretching vibration. d represents the decompression process. (c) Pressure-dependent IR absorbance profiles of two typical gaseous decomposition products during decompression.

tion.[29,30] Indeed, previous high-pressure research on CL-20, a compound notable for its three-dimensional cage structure bearing six nitro groups (-NO_2), consistently demonstrated structural stability without significant chemical reactions up to pressures of approximately 60 GPa.[31−33]

A significant limitation of prior studies is that they have primarily concentrated on static or quasi-hydrostatic compression conditions, paying little attention to the decompression process, implicitly assuming reversibility upon pressure release. Such assumptions may overlook subtle chemical changes, particularly the formation of gaseous decomposition products in minor quantities.

Motivated by these gaps, the current study systematically investigates the chemical reactivity of CL-20 throughout a complete compression−decompression cycle at room temperature, explicitly isolating pressure-induced effects from thermal influences. By combining infrared (IR) spectroscopy sensitive to gaseous products with MD simulations, we specifically explore the impact of mechanical stress gradients (shear stress) under nonhydrostatic ("dry") compression conditions. Our results provide clear experimental evidence that mechanical stress gradients significantly influence chemical decomposition processes in EMs during decompression, offering new insights into the intrinsic sensitivity and reaction mechanisms of energetic materials.

RESULTS AND DISCUSSION

Reaction of CL-20 under Nonhydrostatic Pressure Conditions. Here, we selected ε-CL-20 as the subject of our investigation to study high-pressure chemical reactions. As shown in Figure 1a, the IR spectra of the recovered samples were compared with those of CL-20 before compression (0.3 GPa). The released IR spectrum showed bands at 1750, 2225, and 2340 cm^{-1}, which were assigned to the C═O stretching mode, nitrous oxide (N_2O), and carbon dioxide (CO_2), respectively. In situ high-pressure photographs were obtained to record the color changes of CL-20 under compression. Prior to compression, the sample was white crystals. Upon the complete release of pressure, the color changed from white to yellow-green, indicating a chemical reaction and supporting the results of the IR spectra.

To reveal the chemical reaction in CL-20 during the compression−decompression cycle in more detail, we performed in situ IR experiments under nonhydrostatic pressure conditions up to 30.5 GPa (Figure 1b). The 1800−2200 cm^{-1} range is the absorbance of type II diamond anvil. The IR spectral patterns show no apparent changes upon compression until 30.5 GPa. After decompression from 30.5 to 8.9 GPa, the onset of the reaction is defined by the appearance of two new peaks at about 2339 and 2400 cm^{-1}, which can be attributed to the solid N_2O and solid CO_2, respectively.[34−36] As the pressure decreases, these peaks shift toward a lower wavenumber. Upon total release of pressure, a new broadband appears at about 1750 cm^{-1}, which can be assigned to the stretching vibration of C═O (ν (C═O)). Meanwhile, the two sharp IR peaks of the gaseous decomposition products (N_2O and CO_2) still remain. This could be ascribed to the trapping of these gas molecules by the caged structure of CL-20.[37] Finally, after the cell opens, N_2O and CO_2 gas molecules

https://doi.org/10.1021/jacs.5c06401
J. Am. Chem. Soc. 2025, 147, 24759−24765

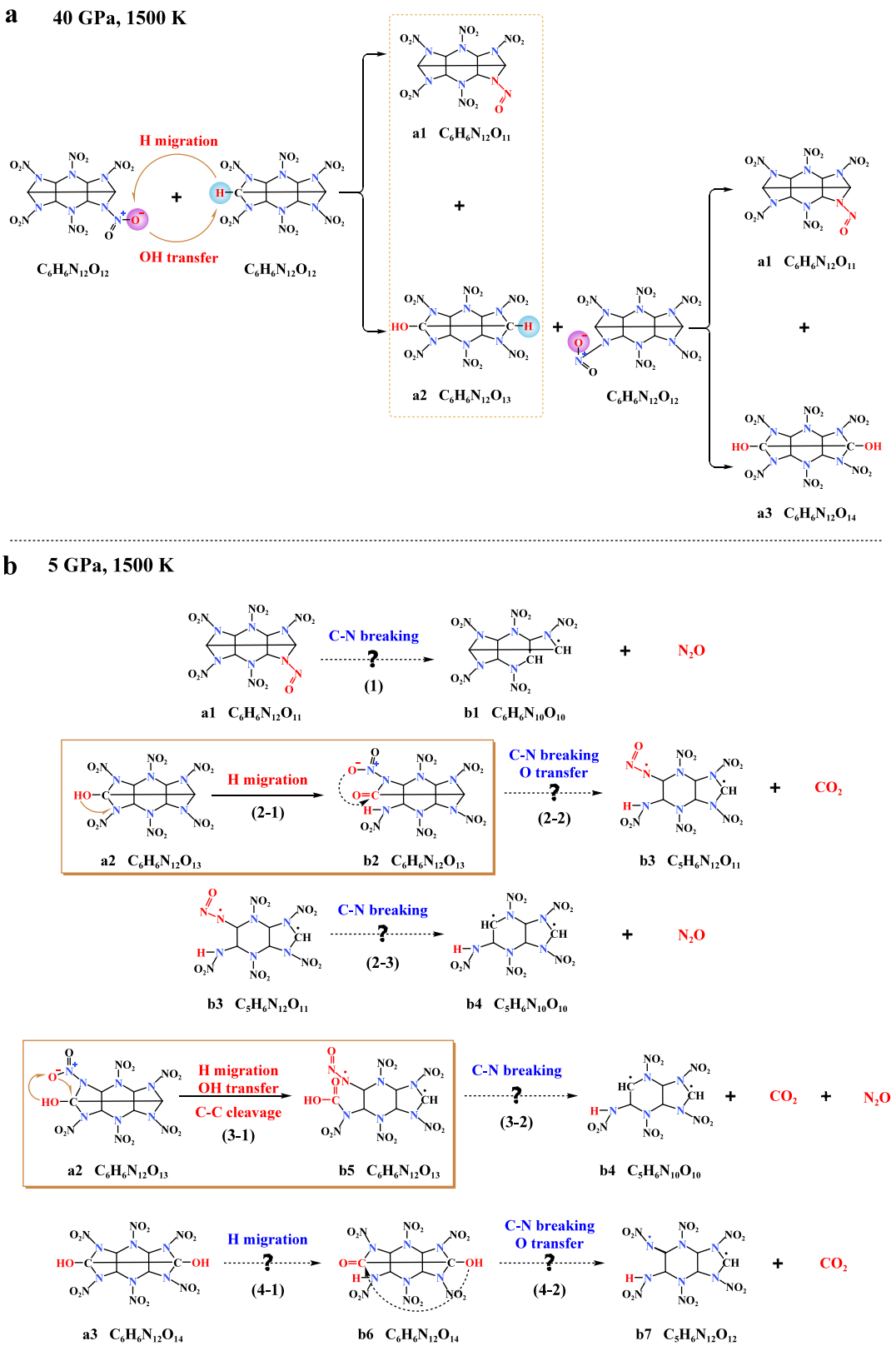

Figure 2. Proposed mechanism of the decompression-induced chemical reaction in CL-20. (a) Bimolecular reaction at high pressure (40 GPa). (b) Reaction pathway decompresses from 40 to 5 GPa. MD simulation supports pathways (2−1) and (3−1). The dotted arrows and question in (b) mark the possible reaction pathways during decompression.

escape from the CL-20 cavity. Figure 1c shows the IR absorbance of N_2O and CO_2 as a function of pressure during the compression−decompression cycle. At a pressure of 8.9 GPa, the reaction occurs, with CO_2 identified as the primary decomposition product. When the sample is decompressed to

https://doi.org/10.1021/jacs.5c06401
J. Am. Chem. Soc. 2025, 147, 24759−24765

ambient pressure, the intensity of the decomposition product CO_2 approaches 1.

We applied a compression of 40.3 GPa to another CL-20 sample. Decompression IR spectra (Figure S2) indicate that, in addition to the production of ν(C═O), N_2O, and CO_2, there are also strongly associated −OH, −NH, or −COOH groups that result in structureless absorption within the 2800−3500 cm^{-1} range. This observation suggests that the reaction degree during decompression is markedly increased with higher peak pressure.

Mechanism of the Decompression-Induced Chemical Reaction. During CL-20's thermal decomposition, IR and mass spectrometry (MS) analysis examined a range of gaseous products, including NO_2, NO, CO, CH_2O, HCN, H_2O, N_2O, and CO_2.[17−19] Decompression-induced chemical reactions in CL-20 were confirmed by IR spectroscopy, which identified N_2O and CO_2 as the only gaseous products. This suggests that the pressure most likely altered the decomposition kinetics of CL-20.

The results of the MD simulation (Figure 2) clearly identify the chemical reaction pathways under pressure. A temperature condition of 1500 K is applied in the simulation to accelerate the reaction. High pressure appears to facilitate bimolecular reactions (Figure 2a), resulting in the formation of various intermediates, including $C_6H_6N_{12}O_{11}$ (a1), $C_6H_6N_{12}O_{13}$ (a2), and $C_6H_6N_{12}O_{14}$ (a3), through H migration and OH transfer reactions. While compression may provide enough energy to initiate a reaction, it also prohibits reactions involving an increase in volume; in other words, only decompression can accelerate gas-generated reactions. MD simulations (Figure 2b) demonstrate that intermediate $C_6H_6N_{12}O_{13}$ (a2) undergoes decompression from 40 to 5 GPa, through H migration resulting in isomer $C_6H_6N_{12}O_{13}$ (b2) or via H migration, OH transfer, and β-scission of the C−C bridge to yield a more stable isomer $C_6H_6N_{12}O_{13}$ (b5). The −C═O, −OH, −NH, and −COOH groups formed in the reaction pathways (2−1) and (3−1) clearly explain the experimental IR spectrum observed during decompression from 40.3 GPa in Figure S2. Also, the intermediates $C_6H_6N_{12}O_{11}$ (a1), $C_6H_6N_{12}O_{14}$ (a3), $C_6H_6N_{12}O_{13}$ (b2), $C_5H_6N_{12}O_{11}$ (b3), and $C_6H_6N_{12}O_{13}$ (b5) further break even more C−N bonds, which makes the final products CO_2 and N_2O. As a whole, MD simulations indicate that chemical reactions occur during the decompression process. However, these reactions are constrained, as they pertain solely to localized groups of CL-20 rather than the entire carbon framework. The observed limitation accounts for the lack of statistically significant change in the diffraction pattern after release (Figure S3). The high pressure inhibits the cleavage of the N-NO_2 bond, leading to the lack of NO_2 formation in both MD simulations and experiments, corroborating previous observations.[38−40] In simple words, high pressure favors the H migration or OH transfer. It prevents the intramolecular N−N bond from breaking, which is the most obvious difference between the reactions at high and atmospheric pressure.

Reaction Threshold Pressure in Different Pressure Environments. To accurately locate the reaction threshold pressure, the pressure was increased or decreased in steps of 0.5−2 GPa in all of the experiments, and the IR spectrum was obtained following pressure stabilization. Because the pressure was applied in stepwise increments, with each step requiring approximately 5 min, the loading process can be considered quasi-isothermal. We recorded the IR spectra of CL-20 under nonhydrostatic compression at room temperature (Figure 3). The saturated peaks at around 1300 and 1590 cm^{-1} can be

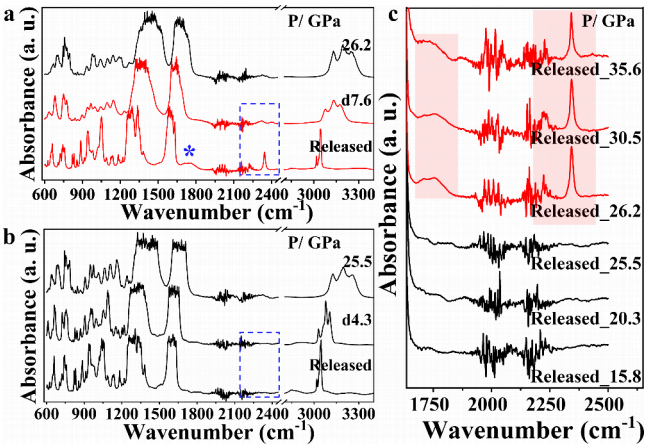

Figure 3. Threshold pressure of the CL-20 chemical reaction under nonhydrostatic compression. Infrared spectral changes of CL-20 after decompression from peak pressures of (a) 26.2 GPa and (b) 25.5 GPa to ambient pressure. The blue asterisk in (a) marks the new peak during CL-20 decompression. (c) Comparison of the IR spectra after release to ambient pressure, with peak pressures of 35.6, 30.5, 26.2, 25.5, 20.3, and 15.8 GPa, respectively.

attributed to the $-NO_2$ stretching vibrations. The IR peaks of the $-NO_2$ stretching vibrations were allowed to become saturated in order to clearly observe the details of the IR peaks of the decomposition products. When decompressed from 26.2 to 7.6 GPa (Figure 3a), the reaction is characterized by a gradual increase in infrared absorption in the range of 2200−2400 cm^{-1} with decreasing pressure, eventually reaching a maximum around 2225 and 2340 cm^{-1}. The subsequent evolution of the spectrum shows that the weak features in the spectrum at 1750 cm^{-1} are connected to ν (C═O), as denoted by a blue asterisk in Figure 3a. After the compression−decompression cycle, the infrared peak intensity of residual CL-20 does not seem to decrease. This means that there is still a lot of unreacted CL-20 in the sample chamber, which is also theoretically supported by the MD simulations.

CL-20 undergoes decompression at 25.5 GPa without initiating a decomposition reaction (Figure 3b). Furthermore, a comparison of the infrared spectra of CL-20 at ambient pressure reveals that decomposition products (N_2O and CO_2) only appear during decompression at peak pressures of 35.6, 30.5, and 26.2 GPa (Figure 3c). Reaching the threshold pressure (26.2 GPa) determines whether the chemical reaction occurs during decompression. Figure S4 displays the infrared spectra for decompression at peak pressures of 35.6, 30.5, and 26.2 GPa. The onset pressures of the reaction at the three peak pressures are 12.8, 8.9, and 7.6 GPa, respectively, indicating a distinct trend. Generally, increasing peak pressure encourages the system to absorb more energy. In the initial decomposition stage, the higher peak pressure is conducive to overcoming the activation energy barrier of C−N bond cleavage earlier, leading to the earlier emergence of decomposition products N_2O and CO_2 in the decompression process.

We assessed the effect of KBr on the reaction pressure threshold and the consequent decomposition products by analyzing the selected IR spectra of CL-20 under hydrostatic pressure conditions of up to 30.1 and 29.2 GPa, using KBr as the PTM at room temperature (Figure 4a,b). The lack of IR

https://doi.org/10.1021/jacs.5c06401
J. Am. Chem. Soc. 2025, 147, 24759−24765

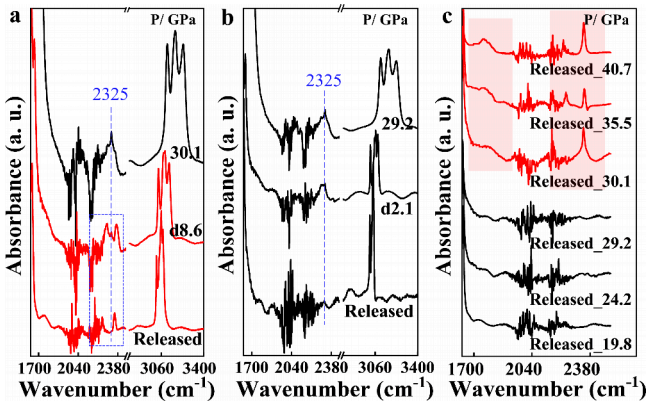

Figure 4. Threshold pressure of the CL-20 chemical reaction under hydrostatic compression with KBr as PTM. The IR spectra of CL-20 up to (a) 30.1 GPa and (b) 29.2 GPa in the range of 1630−3400 cm^{-1}. The dashed line represents the IR peaks of the CO_2 in air at 2325 cm^{-1}. (c) Comparison of the IR spectra after being released to ambient pressure, with peak pressures of 40.7, 35.5, 30.1, 29.2, 24.2, and 19.8 GPa, respectively.

peaks at around 2225 and 2340 cm^{-1} in Figure 4b, which are evident in Figure 4a, indicates that when pressure exceeds the reaction threshold (~30.1 GPa), specific molecules decompose into N_2O and CO_2 during decompression. These features are consistent with the reaction of CL-20 under nonhydrostatic pressure conditions (Figure 3). Figure 4c compares the IR spectra of CL-20 after the compression−decompression cycle. The interference fringes that overlap between the diamond faces and the sample affect the assignment of the observed spectral features in the areas of lower intensity absorption. However, this set of studies indicates that a peak pressure below 30.1 GPa fails to trigger a decompression reaction. Nonhydrostatic pressure (26.2 GPa) and hydrostatic pressure (30.1 GPa, KBr as PTM) exhibit distinct reaction threshold pressures. This may be attributed to the elevated shear stress within the sample chamber under nonhydrostatic circumstances. CL-20 is an anisotropic molecular crystal. Under nonhydrostatic conditions, the anisotropic stress distribution in the sample chamber generates shear stress, inducing local strain and reducing the activation energy for decomposition.[41,42] During decompression, shear stress facilitates the breaking of C−N and C−C bonds in $C_6H_6N_{12}O_{11}$ (a1), $C_6H_6N_{12}O_{13}$ (a2), and $C_6H_6N_{12}O_{14}$ (a3), thereby promoting the formation of CO_2 and N_2O.

Shear Stress in the DAC under Nonhydrostatic Pressure Conditions. The results above show that the pressure environment has no effect on the reaction products of CL-20. However, it significantly impacts the reaction threshold pressure. The elastoplastic differences between materials lead to different shear stress distributions in DACs under pressure. Meade et al.[43] modeled the nonhydrostatic stress state in DACs and demonstrated how pressure gradient at high pressures could provide a reliable estimate of the maximum shear stress across the sample in nonhydrostatic pressure environments. According to the simplified expressions,

$$\frac{dp}{dr} = \frac{2\tau}{h} \quad (1)$$

where p is the mean pressure, r is the radius from the culet center, h is the sample thickness, and τ is the maximum shear stress. Equation 1 demonstrates that a large pressure gradient provides a large shear stress. An increase in shear stress within the sample chamber may lead to a reduction in the reaction threshold pressure.

To conduct Raman mapping of the pressure distribution in a DAC, we used the O−N−O out-of-plane bending at 790 cm^{-1} as the monitored peak (Figure S6), which shifts with pressure up to 31.3 GPa (Figure S5). As the pressure increases, a distinct pressure gradient is evident from the outer edges to the center. Figure S6 shows a high-pressure gradient of 8 at 29.7 GPa. High shear stress can lower the reaction threshold pressure under nonhydrostatic compression (26.2 GPa). Previously, shear stress has been thought to cause chemical reactions in EMs under high pressure.[44] Chemical reactions may become exceedingly intricate when subjected to a combination of shear stress and pressure. To that end, we need to investigate this mechanism further in future work, preferably by combining theoretical and experimental methods.

When 29.7 GPa was released to ambient pressure, a reaction zone labeled 1 appeared in the sample chamber (Figure S7 insert). Line 1 displays the IR spectrum of the decomposition products in zone 1. Comparing line 2, the ν (C═O) (1750 cm^{-1}), N_2O (2225 cm^{-1}), and CO_2 (2340 cm^{-1}) peaks suggest a decomposition reaction has occurred during decompression. According to Figure 3, the pressure in the DAC outer margins is below the reaction threshold (26.2 GPa), which may explain the absence of a decomposition reaction in zone 2.

CONCLUSIONS

In summary, we have demonstrated that pressure alone—serving as a conventional mechanical energy input—can initiate chemical reactions in CL-20 independently of temperature. IR spectroscopy provided definitive evidence of these reactions and clearly identified their gaseous decomposition products. Close packing at high pressures minimizes intermolecular distances and prevents bond cleavage. However, upon decompression from 26.2 GPa under nonhydrostatic ("dry") compression conditions, CL-20 underwent distinct chemical decomposition, producing gaseous species, primarily N_2O and CO_2, which dissipated upon cell opening. MD simulations further revealed detailed reaction pathways, indicating that H migration and OH transfer initiate decomposition, subsequently leading to C−C and C−N bond cleavage during decompression and resulting in the formation of N_2O and CO_2. Remarkably, the chemical decomposition patterns were similar across different hydrostatic conditions, yielding the same gaseous products. Nonetheless, the reaction threshold pressure was significantly lower under non-hydrostatic conditions, underscoring the critical role of shear stress in facilitating chemical bond cleavage.

Overall, our findings demonstrate that pressure-induced chemical reactions can occur in condensed explosives at room temperature. This study validates pressure as an effective alternative initiation factor to temperature for energetic materials (EMs), providing valuable insights for assessing safety risks and informing practical guidelines for the production, pressing, processing, use, and storage of EMs.

ASSOCIATED CONTENT

Supporting Information

The Supporting Information is available free of charge at https://pubs.acs.org/doi/10.1021/jacs.5c06401.

https://doi.org/10.1021/jacs.5c06401
J. Am. Chem. Soc. 2025, 147, 24759−24765

Materials and characterizations, experimental details, computational details, decompression IR spectra, and Raman mapping (PDF)

AUTHOR INFORMATION

Corresponding Authors

Xiao Dong − *Key Laboratory of Weak-Light Nonlinear Photonics and School of Physics, Nankai University, Tianjin 300071, China;* orcid.org/0000-0003-4533-1914; Email: xiao.dong@nankai.edu.cn

Jun Chen − *Laboratory of Computational Physics, Institute of Applied Physics and Computational Mathematics, Beijing 100088, China;* orcid.org/0000-0001-6682-7228; Email: jun_chen@iapcm.ac.cn

Wanghua Chen − *Department of Safety Engineering, Nanjing University of Science and Technology, Nanjing, Jiangsu 210094, China*; Email: chenwh_nust@163.com

Lei Su − *Center for High Pressure Science and Technology Advanced Research, Beijing 100093, China; Shanghai Advanced Research in Physical Sciences, Shanghai 201203, China;* orcid.org/0000-0001-9688-4688; Email: lei.su@sharps.ac.cn

Authors

Xin Zhang − *Department of Safety Engineering, Nanjing University of Science and Technology, Nanjing, Jiangsu 210094, China; Laboratory of Computational Physics, Institute of Applied Physics and Computational Mathematics, Beijing 100088, China; Center for High Pressure Science and Technology Advanced Research, Beijing 100093, China*

Kaiyuan Shi − *Center for High Pressure Science and Technology Advanced Research, Beijing 100093, China*

Jian Xu − *Center for High Pressure Science and Technology Advanced Research, Beijing 100093, China;* orcid.org/0009-0003-6659-2619

Fengyuan Shi − *Key Laboratory of Photochemistry, Institute of Chemistry, University of Chinese Academy of Sciences, Chinese Academy of Sciences, Beijing 100190, China*

Jian Wang − *Center for High Pressure Science and Technology Advanced Research, Beijing 100093, China*

Jiaqing Zhang − *Center for High Pressure Science and Technology Advanced Research, Beijing 100093, China*

Xingbang Dong − *Center for High Pressure Science and Technology Advanced Research, Beijing 100093, China;* orcid.org/0000-0003-3991-4128

Jun Kong − *Center for High Pressure Science and Technology Advanced Research, Beijing 100093, China; Key Laboratory of Weak-Light Nonlinear Photonics and School of Physics, Nankai University, Tianjin 300071, China;* orcid.org/0000-0001-7785-7561

Zhaoxu Du − *Center for High Pressure Science and Technology Advanced Research, Beijing 100093, China*

Haotian Yang − *Center for High Pressure Science and Technology Advanced Research, Beijing 100093, China*

Complete contact information is available at: https://pubs.acs.org/10.1021/jacs.5c06401

Author Contributions

[▽]X.Z., K.S., J.X., and F.S. have equal contributions to this work.

Notes

The authors declare no competing financial interest.

ACKNOWLEDGMENTS

This work was supported by the Advanced Materials-National Science and Technology Major Project (No. 2024ZD0607000) and the National Natural Science Foundation of China (No. 21627802). The authors gratefully acknowledge the use of resources at the BL15U1 Station and BL17UM Station, Shanghai Synchrotron Radiation Facility. L.S. acknowledges the financial support from Shanghai Key Laboratory of MFree, China (No. 22dz2260800) and Shanghai Science and Technology Committee, China (No. 22JC1410300).

REFERENCES

(1) Benz, M.; Klapotke, T. M.; Stierstorfer, J.; Voggenreiter, M. Synthesis and Characterization of Binary, Highly Endothermic, and Extremely Sensitive 2,2'-Azobis(5-azidotetrazole). *J. Am. Chem. Soc.* **2022**, *144* (14), 6143−6147.

(2) Gao, H.; Shreeve, J. M. Azole-based energetic salts. *Chem. Rev.* **2011**, *111* (11), 7377−7436.

(3) Sikder, A. K.; Sikder, N. A review of advanced high performance, insensitive and thermally stable energetic materials emerging for military and space applications. *J. Hazard. Mater.* **2004**, *112* (1−2), 1−15.

(4) Zhang, C.; Wang, X.; Huang, H. π-Stacked Interactions in Explosive Crystals: Buffers against External Mechanical Stimuli. *J. Am. Chem. Soc.* **2008**, *130* (26), 8359−8365.

(5) Kuklja, M. M.; Rashkeev, S. N. Shear-strain-induced structural and electronic modifications of the molecular crystal 1, 1-diamino-2, 2-dinitroethylene: Slip-plane flow and band gap relaxation. *Phys. Rev. B* **2007**, *75* (10), No. 104111.

(6) Kuklja, M. M.; Rashkeev, S. N. Self-accelerated mechanochemistry in nitroarenes. *J. Phys. Chem. Lett.* **2010**, *1* (1), 363−367.

(7) Liu, J.; Yang, J.; Zhu, G.; Li, J.; Li, Y.; Zhai, Y.; Song, H.; Yang, Y.; Li, H. Revealing the Ultrafast Energy Transfer Pathways in Energetic Materials: Time-Dependent and Quantum State-Resolved. *JACS Au.* **2024**, *4* (11), 4455−4465.

(8) Sharia, O.; Kuklja, M. M. Rapid materials degradation induced by surfaces and voids: ab initio modeling of β-octatetramethylene tetranitramine. *J. Am. Chem. Soc.* **2012**, *134* (28), 11815−11820.

(9) Yan, T.; Yang, H.; Yang, C.; Yi, Z.; Zhu, S.; Cheng, G. An advanced and applicable heat-resistant explosive through controllable regiochemical modulation. *J. Mater. Chem. A* **2020**, *8* (45), 23857−23865.

(10) You, S.; Chen, M. W.; Dlott, D. D.; Suslick, K. S. Ultrasonic hammer produces hot spots in solids. *Nat. Commun.* **2015**, *6* (1), 6581.

(11) Allen, J. E.; Zybin, S. V.; Morozov, S. I.; O'Sullivan, O. T.; Kawamura, C.; Waxler, D. E.; Hooper, J. P.; Goddard, W. A., Iii; Zdilla, M. J. High-Energy-Density Material with Magnetically Modulated Ignition. *J. Am. Chem. Soc.* **2024**, *146* (7), 4500−4507.

(12) Millar, D. I. *Energetic Materials at Extreme Conditions*. Springer Science & Business Media, 2011.

(13) Mao, H.-K.; Ji, C.; Li, B.; Liu, G.; Gregoryanz, E. Extreme Energetic Materials at Ultrahigh Pressures. *Engineering.* **2020**, *6* (9), 976−980.

(14) Fabbiani, F. P.; Pulham, C. R. High-pressure studies of pharmaceutical compounds and energetic materials. *Chem. Soc. Rev.* **2006**, *35* (10), 932−942.

(15) Naik, N.; Gore, G.; Gandhe, B.; Sikder, A. Studies on thermal decomposition mechanism of CL-20 by pyrolysis gas chromatography−mass spectrometry (Py-GC/MS). *J. Hazard. Mater.* **2008**, *159* (2−3), 630−635.

(16) Zhu, Y.; Zhou, Z.; Ye, L.; Yuan, W.; Xiao, L.; Qu, W.; Cui, C.; Chen, X.; Ren, H.; Cai, J. Direct mass spectrometric observation and reaction mechanism of gas-phase initial intermediates during CL-20 decomposition. *Combust. Flame* **2022**, *241*, No. 112095.

(17) Okovytyy, S.; Kholod, Y.; Qasim, M.; Fredrickson, H.; Leszczynski, J. The Mechanism of Unimolecular Decomposition of 2, 4, 6, 8, 10, 12-Hexanitro-2, 4, 6, 8, 10, 12-hexaazaisowurtzitane. A Computational DFT Study. *J. Phys. Chem. A* **2005**, *109* (12), 2964−2970.
(18) Song, X.; Wang, Y.; Zhao, S.; Li, F. Mechanochemical fabrication and properties of CL-20/RDX nano co/mixed crystals. *RSC advances.* **2018**, *8* (59), 34126−34135.
(19) Wen, M.; Chang, X.; Xu, Y.; Chen, D.; Chu, Q. Determining the mechanical and decomposition properties of high energetic materials (α-RDX, β-HMX, and ε-CL-20) using a neural network potential. *Phys. Chem. Chem. Phys.* **2024**, *26* (13), 9984−9997.
(20) Zhou, J.; Ding, L.; Zhu, Y.; Wang, B.; Li, X.; Zhang, J. Comparative thermal research on tetraazapentalene-derived heat-resistant energetic structures. *Sci. Rep.* **2020**, *10* (1), 21757.
(21) Liu, G.; Xiong, Y.; Gou, R.; Zhang, C. Difference in the thermal stability of polymorphic organic crystals: A comparative study of the early events of the thermal decay of 2, 4, 6, 8, 10, 12-hexanitro-2, 4, 6, 8, 10, 12-hexaazaisowurtzitane (CL-20) polymorphs under the volume constraint condition. *J. Phys. Chem. C* **2019**, *123* (27), 16565−16576.
(22) Song, Q.; Zhang, L.; Mo, Z. Alleviating the stability−performance contradiction of cage-like high-energy-density materials by a backbone-collapse and branch-heterolysis competition mechanism. *Phys. Chem. Chem. Phys.* **2022**, *24* (32), 19252−19262.
(23) Wang, F.; Chen, L.; Geng, D.; Lu, J.; Wu, J. Chemical reactions of a CL-20 crystal under heat and shock determined by ReaxFF reactive molecular dynamics simulations. *Phys. Chem. Chem. Phys.* **2020**, *22* (40), 23323−23332.
(24) Ceppatelli, M.; Santoro, M.; Bini, R.; Schettino, V. Fourier transform infrared study of the pressure and laser induced polymerization of solid acetylene. *J. Chem. Phys.* **2000**, *113* (14), 5991−6000.
(25) Ciabini, L.; Santoro, M.; Bini, R.; Schettino, V. High pressure reactivity of solid benzene probed by infrared spectroscopy. *J. Chem. Phys.* **2002**, *116* (7), 2928−2935.
(26) Ceppatelli, M.; Santoro, M.; Bini, R.; Schettino, V. High pressure reactivity of solid furan probed by infrared and Raman spectroscopy. *J. Chem. Phys.* **2003**, *118* (3), 1499−1506.
(27) Citroni, M.; Ceppatelli, M.; Bini, R.; Schettino, V. The high-pressure chemistry of butadiene crystal. *J. Chem. Phys.* **2003**, *118* (4), 1815−1820.
(28) Chelazzi, D.; Ceppatelli, M.; Santoro, M.; Bini, R.; Schettino, V. Pressure-induced polymerization in solid ethylene. *J. Phys. Chem. B* **2005**, *109* (46), 21658−21663.
(29) Gao, C.; Zhang, X.; Zhang, C.; Sui, Z.; Hou, M.; Dai, R.; Wang, Z.; Zheng, X.; Zhang, Z. Effect of pressure gradient and new phases for 1,3,5-trinitrohexahydro-s-triazine (RDX) under high pressures. *Phys. Chem. Chem. Phys.* **2018**, *20* (21), 14374−14383.
(30) Sui, Z.; Sun, X.; Liang, W.; Dai, R.; Wang, Z.; Huang, S.; Zheng, X.; Zhang, Z.; Wu, Q. Phase confirmation and equation of state of β-HMX under 40 GPa. *J. Phys. Chem. C* **2019**, *123* (50), 30121−30128.
(31) Ciezak, J. A.; Jenkins, T. A.; Liu, Z. Evidence for a High-Pressure Phase Transition of ε-2, 4, 6, 8, 10, 12-Hexanitrohexaazaisowurtzitane (CL-20) Using Vibrational Spectroscopy. *Propellants, Explos, Pyrotech.* **2007**, *32* (6), 472−477.
(32) Konar, S.; Hunter, S.; Morrison, C. A.; Coster, P. L.; Maynard-Casely, H. E.; Richardson, J. G.; Marshall, W. G.; Kleppe, A.; Parker, S. F.; Pulham, C. R. High-pressure neutron powder diffraction study of ε-cl-20: a gentler way to study energetic materials. *J. Phys. Chem. C* **2020**, *124* (51), 27985−27995.
(33) Sun, X.; Sui, Z.; Wang, J.; Li, X.; Wang, X.; Dai, R.; Wang, Z.; Huang, S.; Zhang, Z. Phase Transition Routes for ε-and γ-CL-20 Crystals under High Pressures of up to 60 GPa. *J. Phys. Chem. C* **2020**, *124* (9), 5061−5068.
(34) Iota, V.; Park, J.; Yoo, C. Phase diagram of nitrous oxide: Analogy with carbon dioxide. *Phys. Rev. B* **2004**, *69* (6), No. 064106.
(35) Scelta, D.; Dziubek, K. F.; Ende, M.; Miletich, R.; Mezouar, M.; Garbarino, G.; Bini, R. Extending the stability field of polymeric carbon dioxide phase V beyond the Earth's geotherm. *Phys. Rev. L.* **2021**, *126* (6), No. 065701.
(36) Li, J.; Sode, O.; Voth, G. A.; Hirata, S. A solid−solid phase transition in carbon dioxide at high pressures and intermediate temperatures. *Nat. Commun.* **2013**, *4* (1), 2647.
(37) Jin, D.; Xu, J.; Zhang, H.; Lei, M.; Sun, J. Comparative Study of Experiments and Calculations on the Guest Molecules' Escaping Mechanism of CL-20-Based Host−Guest Energetic Materials. *J. Phys. Chem. C* **2023**, *127* (24), 11641−11651.
(38) Wang, F.; Chen, L.; Geng, D.; Lu, J.; Wu, J. Effect of density on the thermal decomposition mechanism of ε-CL-20: a ReaxFF reactive molecular dynamics simulation study. *Phys. Chem. Chem. Phys.* **2018**, *20* (35), 22600−22609.
(39) Song, Z.-Q.; Zhang, H.-R.; Nie, H.; Liu, Y.; Yan, Q.-L. Research progress on thermal reactivity and thermolysis mechanisms of CL-20. *J. Anal. Appl. Pyrolysis.* **2024**, *179*, No. 106508.
(40) Wang, F.; Chen, L.; Geng, D.; Lu, J.; Wu, J. Molecular dynamics simulations of an initial chemical reaction mechanism of shocked CL-20 crystals containing nanovoids. *J. Phys. Chem. C* **2019**, *123* (39), 23845−23852.
(41) Kim, D.; Oh, S.; Yi, S.; Bae, S.; Moon, S. Preparation of Indium−Tin Oxide Particles in Shear-Induced Multilamellar Vesicles (Spherulites) as Chemical Reactors. *Chem. Mater.* **2000**, *12* (4), 996−1002.
(42) Nadeem, I.; Ambrožič, B.; Dražić, G.; Kovač, J.; Cavaleiro, A.; Kalin, M. Super-low friction and wear in steel contacts enabled by tribo-induced structural degradation of graphene quantum dots. *Mater. Des.* **2024**, *244*, No. 113111.
(43) Meade, C.; Jeanloz, R. Yield strength of MgO to 40 GPa. *J. Geophys. Res.* **1988**, *93* (B4), 3261−3269.
(44) Yoo, C. S.; Cynn, H. Equation of state, phase transition, decomposition of β-HMX (octahydro-1, 3, 5, 7-tetranitro-1, 3, 5, 7-tetrazocine) at high pressures. *J. Chem. Phys.* **1999**, *111* (22), 10229−10235.

https://doi.org/10.1021/jacs.5c06401
J. Am. Chem. Soc. 2025, 147, 24759−24765